Radiotherapy and Oncology 138 (2019) 158–165

Contents lists available at ScienceDirect

Radiotherapy and Oncology

journal homepage: www.thegreenjournal.com

Original Article

Evaluating the benefit of PBS vs. VMAT dose distributions in terms of dosimetric sparing and robustness against inter-fraction anatomical changes for pediatric abdominal tumors

Filipa Guerreiro [a,*], Cornel Zachiu [a], Enrica Seravalli [a], Cássia O. Ribeiro [b], Geert O. Janssens [c,d], Mario Ries [e], Baudouin Denis de Senneville [e,f], John H. Maduro [b], Charlotte L. Brouwer [b], Erik W. Korevaar [b], Antje C. Knopf [b], Bas W. Raaymakers [a]

[a] Department of Radiotherapy, University Medical Center Utrecht; [b] Department of Radiation Oncology, University Medical Center Groningen, University of Groningen; [c] Department of Radiation Oncology, University Medical Center Utrecht; [d] Princess Máxima Center for Paediatric Oncology, Utrecht; [e] Imaging Division, University Medical Center Utrecht, The Netherlands; and [f] Institut de Mathématiques de Bordeaux, University of Bordeaux, France

ARTICLE INFO

Article history:
Received 18 February 2019
Received in revised form 27 May 2019
Accepted 17 June 2019
Available online 11 July 2019

Keywords:
Pediatric IGRT
Pediatric abdominal tumors
Robust pencil beam scanning
Proton therapy
VMAT
Inter-fraction anatomical changes

ABSTRACT

Background and purpose: To evaluate the dosimetric sparing and robustness against inter-fraction anatomical changes between photon and proton dose distributions for children with abdominal tumors.
Material and methods: Volumetric modulated arc therapy (VMAT) and intensity-modulated pencil beam scanning (PBS) proton dose distributions were calculated for 20 abdominal pediatric cases (average 3, range 1–8 years). VMAT plans were based on a full-arc while PBS plans on 2–3 posterior-oblique irradiation fields. Plans were robustly optimized on a patient-specific internal target volume (ITV) using a uniform 5 mm set-up uncertainty. Additionally, for the PBS plans a ± 3% proton range uncertainty was accounted for. Fractional dose re-calculations were performed using the planning computed tomography (CT) deformably registered to the daily cone-beam CT (CBCT) images. Fractional doses were accumulated rigidly. Planned and CBCT accumulated VMAT and PBS dose distributions were compared using dose–volume histogram (DVH) parameters.
Results: Significant better sparing of the organs at risk with a maximum reduction in the mean dose of 40% was achieved with PBS. Mean ITV DVH parameters differences between planned and CBCT accumulated dose distributions were smaller than 0.5% for both VMAT and PBS. However, the ITV coverage ($V_{95\%}$ > 99%) was not reached for one patient for the accumulated VMAT dose distribution.
Conclusions: For pediatric patients with abdominal tumors, improved dosimetric sparing was obtained with PBS compared to VMAT. In addition, PBS delivered by posterior-oblique irradiation fields demonstrated to be robust against anatomical inter-fraction changes. Compared to PBS, daily anatomical changes proved to affect the target coverage of VMAT dose distributions to a higher extent.
 Radiotherapy and Oncology 138 (2019) 158–165

Wilms' tumor (WT) and neuroblastoma (NBL) belong to the most frequent abdominal tumors in pediatric patients [1,2]. Due to the use of a multimodality treatment comprising surgery, chemotherapy and radiotherapy, the survival rates for these patients have increased over the past few decades [3,4]. The subgroup of patients that receive radiotherapy is however at increased risk of developing toxicity to the normal tissue (NT).

With the use of more advanced photon radiotherapy techniques, such as volumetric modulated arc therapy (VMAT), conformal dose gradients are delivered to complex target volumes enabling the reduction of the NT volume irradiated at tumor dose levels [5]. Nevertheless, low doses are still widely spread in the surrounding NT. With intensity-modulated proton therapy (IMPT) using a pencil beam scanning (PBS) delivery, as a result of the unique dose-deposition pattern characterized by the low entrance dose and rapid dose fall-off [6,7], there is hope to reduce the low dose bath and consequently the radiation-induced late effects [8]. In literature, clinical studies on PBS are sparse, patient cohorts are small and the follow-up is too short to evaluate long-term

* Corresponding author at: Department of Radiotherapy, University Medical Center Utrecht, Heidelberglaan 100, HP: Q.02.2.312, 3584 CX Utrecht, The Netherlands.
E-mail addresses: F.Guerreiro@umcutrecht.nl (F. Guerreiro), C.Zachiu@umcutrecht.nl (C. Zachiu), E.Seravalli@umcutrecht.nl (E. Seravalli), c.oraboni.ribeiro@umcg.nl (C.O. Ribeiro), G.O.R.Janssens@umcutrecht.nl (G.O. Janssens), M.Ries@umcutrecht.nl (M. Ries), b.desenneville@umcutrecht.nl (B.D. de Senneville), j.h.maduro@umcg.nl (J.H. Maduro), c.l.brouwer@umcg.nl (C.L. Brouwer), e.w.korevaar@umcg.nl (E.W. Korevaar), a.c.knopf@umcg.nl (A.C. Knopf), b.w.raaymakers@umcutrecht.nl (B.W. Raaymakers).

https://doi.org/10.1016/j.radonc.2019.06.025
0167-8140/

complications. However, publications assessing the dosimetric feasibility of treating pediatric abdominal tumors with PBS report a better NT sparing with this type of irradiation [9–12].

During radiotherapy treatments in abdominal cancer, inter-fraction anatomical changes, such as patient diameter variations, due to weight loss/gain, and daily gastrointestinal gas volume differences, might occur. Due to the unpredictability of these changes over the treatment course and the difference between the depth-dose curves of photons and protons, the effect of inter-fraction uncertainties on the target and NT doses can be different between the two delivery techniques. In theory, proton dose distributions are more sensitive to uncertainties in computed tomography (CT) densities and changes in patient anatomy compared to photon dose distributions [13]. Robust treatment planning is currently used in proton radiotherapy to prevent that the target coverage is not maintained throughout the treatment by mitigating the effect of both range and set-up uncertainties [14–17].

To facilitate the choice between photons and protons to treat pediatric patients, a dosimetric comparison and an evaluation of the robustness of both delivery techniques should be performed. However, studies comparing the robustness of photon and proton delivery modalities against inter-fraction anatomical changes for children have not been published yet. The goal of this study was to quantify for pediatric abdominal tumors: (1) the dosimetric differences in terms of dose sparing and (2) the dosimetric impact of daily anatomical changes based on cone-beam CT (CBCT) information between VMAT, used clinically at our department, and intensity-modulated PBS dose distributions.

Materials and methods

Patient and imaging characteristics

After institutional review board approval (WAG/mb/17/008865), data from 20 consecutive patients treated at our department between April 2015 and September 2017 were included in this study: 9 WT patients (average: 3, range 1–8 years), undergoing flank irradiation after nephrectomy, and 11 NBL patients (average: 4, range 1–7 years) (Supplementary material).

For treatment preparation, patients were fixated in a vacuum mattress (Bluebag, Elekta, Stockholm, Sweden) in a supine position with the arms wide along the body. A 4-dimensional CT (4D-CT) was acquired for each patient in treatment position and using the same field of view (FOV): from the lungs until the lower abdomen. The 4D-CT images were obtained as a series of 10 phases using a 16-, 40-, or 64-channel detector scanner (Brilliance, Philips Medical Systems, Best, The Netherlands). Scans with a current of 120 mA, with 90 kV, a pitch of 0.8, a gantry rotation speed of 0.7 s, a slice thickness of 3 mm corresponding to a CT dose index (CTDI) of 6 mGy were acquired. The planning-CT was obtained by taking the pixel-by-pixel average of the 10 phases of the 4D-CT. During treatment, daily CBCT images were acquired for all treatment fractions using the XVI 4.5.1 on-board CBCT imaging system (Elekta, Stockholm, Sweden). Scans with an arc of 200° of 10 ms and 16 mA with 100 kV and an acquisition timeframe of 30 s, leading to four times less imaging dose than a standard adult pre-set (CTDI of 1 mGy), were taken. During treatment, each CBCT was registered to the planning-CT using the rigid registration algorithm available online on the XVI software (Elekta, Stockholm, Sweden) [18,19].

Treatment planning characteristics

The clinical target volume (CTV) was created by expanding the gross tumor volume (GTV) by 5 mm for the NBL patients and 10 mm for the WT patients. To account for the breathing motion, an internal target volume (ITV) was individualized for each patient and orthogonal direction. Breathing motion was assessed by measuring center of mass displacements of surgical clips, used as surrogates for the tumor bed boundaries, visible on the maximum expiration and inspiration phases of the 4D-CT image. ITV expansions were up to 1 mm in the left–right (LR) and anterior–posterior (AP) directions and up to 2 mm in the cranio-caudal (CC) direction, depending on the patient [20]. All organs at risk (OARs) were contoured using the planning-CT. In addition, patient-specific safety margins were added to the OARs contours according to the individual motion measured on the 4D-CT image. OARs margins were up to 1 mm in the LR and AP directions and up to 3 mm in the CC direction, depending on the organ and on the patient [20].

3D treatment plan optimization was performed in RayStation software (Raysearch, Stockholm, Sweden) using the planning-CT and using a collapsed cone engine for VMAT and a pencil beam algorithm for intensity-modulated PBS dose distributions [21]. According to the department clinical protocol, VMAT plans consisted of a full-arc. Given the posterior location of the tumor, 2 to 3 posterior irradiation fields were selected for the PBS plans. Number and direction of the proton beams (range [90°, 240°]) were chosen individually per patient according to the tumor location and achievement of planning goals. To cover shallow targets, a range shifter of 40 mm was used. Additionally, a relative biological effectiveness (RBE) of 1.1 was included [21,22]. For PBS dose calculations, the Monte Carlo dose engine is known to be more accurate than the pencil beam algorithm [23]. Nevertheless, due to the posterior location of the target and the chosen beam configuration, an average uncertainty of 0.5% on the dose–volume histogram (DVH) parameters was found between Monte Carlo and pencil beam optimized PBS dose distributions. Given this negligible difference and the longer optimization time required by the Monte Carlo engine, PBS plans were computed using the pencil beam algorithm.

The center of the ITV was defined as the isocenter for both modalities. The prescribed dose (PD) ranged from 14.4 to 36.0 Gy (from 8 to 20 fractions), depending on the patient (Supplementary material). To reduce the risk of asymmetric skeletal growth, a homogeneous dose was aimed for the vertebra volume adjacent to the ITV for both modalities: $V_{70\%-80\%} > 95–98\%$, depending on the patient [24].

To assure a fair dosimetric comparison, both VMAT and PBS dose distributions were 3D ITV-based robustly optimized and evaluated accounting for several scenarios where patient set-up and range (only for PBS) uncertainties were simulated [21]. Set-up uncertainties were modeled by making translational shifts of the plan isocenter and range uncertainties by scaling the planning-CT density. A uniform 5 mm patient set-up and ± 3% range uncertainties were accounted for [13,25]. During 3D robust plan optimization, robustness against these uncertainties was attained using a minimax optimization method [14,21]. Plans were optimized accounting for different dose scenarios using the selected set-up (5 mm in 6 directions plus nominal plan) and range (± 3% plus nominal plan, only for PBS) uncertainties. In total, 7 and 21 dose scenarios were calculated during the VMAT and PBS plan optimization, respectively. For the 3D robust plan evaluation, different dose scenarios were computed using the same magnitude of the set-up (5 mm in 26 fixed directions) and range (± 3%, only for PBS) uncertainties. In total, 26 and 52 dose scenarios were calculated for the VMAT and PBS plans, respectively. The information from all scenarios per technique was combined in a voxel-wise minimum evaluation dose (Vw_{min}) by calculating the minimum dose per voxel in all scenarios. Plans were considered clinically robust if 98% of the ITV received at least 95% of the PD ($V_{95\%} > 98\%$) in the Vw_{min} [26].

As a result of the proton finite range and stopping power sensitivity to electron density variations, the robustness of the planned PBS dose distributions may be compromised by small deviations

occurring during treatment delivery, such as (1) patient anatomy changes due to breathing motion, (2) inter-play effects and (3) machine errors [27]. Therefore, to assure that for this patient group a 3D ITV-based robust optimization is sufficient to cover these disturbing effects (1–3), a 4D robustness evaluation method (4DREM) was used to evaluate the PBS dose distribution of the patient denoting the largest target breathing motion (2 mm in the CC direction) [28]. Disturbing effects were considered by calculating sub-plan doses, based on treatment-plan specific delivery-machine log files, on all 10 phases of the 4D-CT image [28]. Phase-specific dose contributions were accumulated on the expiration phase using ANACONDA (Anatomically Constrained Deformation Algorithm) algorithm available in RayStation software [21]. Additionally, for each sub-plan, set-up and range uncertainties were incorporated by calculating dose scenarios accounting for 5 mm isocenter shifts in 14 directions and planning-CT density perturbations of ± 3%. PBS plan robustness was evaluated by calculating a 4D accumulated Vw_{min} (4D Vwa_{min}) obtained from the computed phase-specific dose scenarios. Robustness was confirmed if 98% of the CTV received at least 95% of the PD ($V_{95\%}$ > 98%) in the 4D Vwa_{min}.

Fractional dose calculation and accumulation

Fractional dose re-calculations were performed using the daily CBCT images. Despite CBCT is commonly employed for patient position verification during treatment, the imaging quality is inferior compared to CT resulting in incorrect Hounsfield units (HUs) for dose calculations [29–31]. For the estimation of the HUs from the CBCTs, the planning-CT was deformably registered to each CBCT using Evolution [32]. This algorithm was previously validated for CT-CBCT registrations for kidney and lung cancer patients [33]. The performance of the registration algorithm was evaluated by visual inspection of tissue landmarks (e.g surgical clips). On the deformed CTs (dCTs), the gas volumes from the planning-CT were filled with a water equivalent density (0 HU) and the gas volumes from the CBCTs were rigidly copied for dose calculation purposes. Fractional doses were re-calculated on the dCTs and accumulated rigidly on the planning-CT. A rigid dose accumulation was chosen due to the limited soft-tissue contrast seen on the CBCTs (Fig. 1). As CBCT images were acquired with less imaging dose than a standard adult protocol (Section 'Patient and imaging characteristics'), an accurate estimation of the daily deformations cannot be guaranteed for all structures. Thus, the clinical ITV and OARs, delineated on the planning-CT, were used for the planned and CBCT accumulated dose distributions evaluation.

Evaluation

Anatomy

The changes in patient diameter and in gastrointestinal gas volume on the planning-CT and CBCTs were calculated for each patient. Gastrointestinal gas pockets were delineated within the available CBCT FOV. Variations in patient diameter were assessed by computing the difference of the distance in the AP direction of the ITV center of mass to the patient's surface between the planning-CT and the CBCT images.

Dosimetry

Two separate evaluations were performed: (1) comparison between VMAT and PBS planned dose distributions in terms of ITV robustness and dose sparing and (2) comparison between planned and CBCT accumulated VMAT and PBS dose distributions in terms of ITV robustness, OARs and NT doses.

For both (1) and (2), clinical DVH parameters were evaluated. For the ITV, the $D_{98\%}$, $D_{50\%}$, and $D_{2\%}$ were computed. In addition, the $V_{95\%}$ was calculated in the Vw_{min} and in the CBCT accumulated Vw_{min} (CBCT Vwa_{min}) to evaluate the robustness of planned (1) and accumulated (2) dose distributions, respectively. CBCT Vwa_{min} was obtained using a 1 mm set-up uncertainty (in 26 fixed directions), to simulate residual treatment errors, and a ± 3% range uncertainty (only for PBS). For the OARs, mean dose (D_{mean}), $D_{50\%}$ and $D_{2\%}$ were computed. For the NT (defined as the body minus the ITV), D_{mean}, V_{2Gy} and $V_{95\%}$ were calculated. Comparisons were statistically evaluated using the Wilcoxon signed-rank test ($p < 0.05$).

Results

Anatomy

In total, 224 CBCTs were evaluated. Patient diameter variations between the planning-CT and CBCTs were on average 0.5 ± 0.4 cm (range [−1.2; 2.0] cm). The volume of gastrointestinal gas as seen on the CBCT images showed large differences compared to the planning-CT: average 99.4 ± 126.9 ml (range [−216.7; 454.7] ml).

Dosimetry

ITV coverage was fulfilled in the planned VMAT and PBS dose distributions. Mean $V_{95\%}$ in the Vw_{min} was 98.7% ± 0.5% (range [98.2%; 99.8%]) and 98.8% ± 0.6% (range [98.1%; 99.6%]) for VMAT and PBS dose distributions, respectively. For the patient denoting the largest breathing motion, the $V_{95\%}$ of the CTV was 99.8% in the 4D Vwa_{min}. Significant better sparing of the OARs and NT was achieved with PBS when compared to VMAT for all patients (Table 1, Fig. 2). The average reduction in the D_{mean} was 12.9 ± 8.0% (range [3.4%; 33.1%]) for the contralateral kidney, 8.1 ± 4.5% (range [2.0%; 15.7%]) for the ipsilateral kidney, 22.8 ± 7.4% (range [5.5%; 34.8%]) for the liver, 13.4 ± 7.7% (range [1.6%; 28.9%]) for the spleen, 17.4 ± 10.5% (range [3.8%; 39.5%]) for the pancreas and 8.0 ± 2.6% (range [3.7%; 13.9%]) for the NT.

Significant differences between the planned and CBCT accumulated dose distributions were only found for the ITV on the VMAT plans (Table 2). For the accumulated VMAT dose distributions, the ITV coverage was not met for one patient due to the large variation of gas volumes between the planning-CT and the CBCT images (Fig. 3). Smaller dose differences on the ITV were found between planned and accumulated PBS dose distributions (Table 2, Fig. 3). Mean $V_{95\%}$ in the CBCT Vwa_{min} was 99.6% ± 0.8% (range [96.8%; 100%]) and 99.8% ± 0.3% (range [99.1%; 100%]) for VMAT and PBS dose distributions, respectively. For the OARs, mean differences between planned and CBCT accumulated dose distributions were below 1.9% for VMAT and below 0.6% for PBS. Moreover, larger individual differences were found for VMAT (range [-11.3%; 9.6%]) compared to PBS (range [-5.3%; 5.2%]) dose distributions (Table 2).

Discussion

In the present study, dosimetric differences between 3D ITV-based robustly optimized VMAT and intensity-modulated PBS dose distributions were quantified in 20 pediatric patients with abdominal cancer. Moreover, the robustness of VMAT and PBS dose distributions against inter-fraction anatomical changes (<2 cm, <455 ml), visualized on daily CBCT images, was investigated for the same patient group. Results demonstrate a significant dosimetric sparing of the OARs and NT without compromising the target dose with PBS for all patients. Furthermore, PBS delivered by posterior-oblique irradiation fields proved to be more robust against daily anatomical inter-fraction changes compared to VMAT using a full-arc delivery.

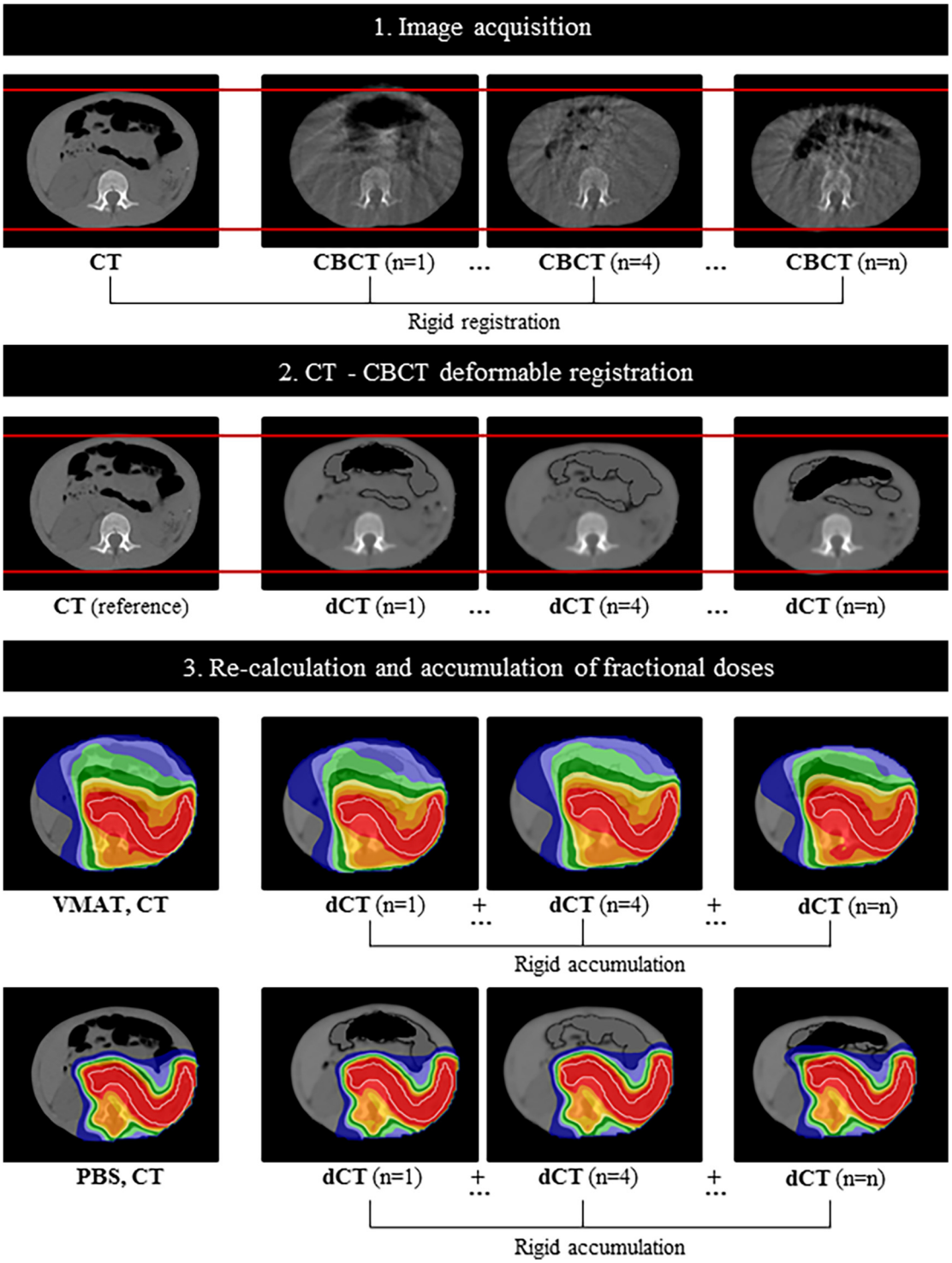

Fig. 1. Schematic representation of the workflow used in this study. For the image acquisition (1), a planning-CT and daily CBCTs were acquired for each patient. CBCT images were obtained online for all treatment fractions and rigidly registered to the planning-CT. For the fractional dose re-calculations, the planning-CT was deformably registered to the CBCT images (2). Fractional doses were re-calculated on the dCTs and accumulated rigidly on the planning-CT for both VMAT and PBS dose distributions (3).

In literature, the dosimetric sparing with PBS was already investigated for both WT and NBL patients against conventional radiotherapy using two opposing fields [9,12], 3D conformal radiotherapy [11] and intensity-modulated radiation therapy (IMRT) [9,10]. Nevertheless, none of these studies compared PBS against VMAT. In addition, none of them used robust optimization and evaluation to account for the effect of both set-up and range uncertainties on the PBS dose distributions limiting the generality of the comparison between approaches. In proton therapy, uncertainties in CT densities and patient anatomy can generate severe effects on the delivered dose as proton path length changes result in displacements of the Bragg peak dose fall-off [34,35]. Consequently, a PTV-based plan optimization is not accurate enough for proton therapy [35,36]. In the present study, ITV-based robustly optimized VMAT plans were chosen for the comparison with PBS to mitigate biases related to the use of different optimization

Table 1
DVH parameters (%) comparison of VMAT and PBS dose distributions, with $p < 0.05$ (Wilcoxon signed-rank test) considered significant (in bold). ΔD denotes the difference between VMAT and PBS dose distributions. Values are presented as a percentage of the respective PD. *Abbreviations: SD = standard deviation.*

Structures	Parameter	VMAT	PBS	ΔD (VMAT–PBS)		
		mean ± SD (%)	mean ± SD (%)	mean ± SD (%)	range (%)	p
ITV	$D_{98\%}$	98.1 ± 0.5	98.1 ± 0.5	0.0 ± 0.8	[−1.2; 1.5]	1.0
	$D_{50\%}$	100.2 ± 0.1	100.4 ± 0.2	−0.2 ± 0.2	[−0.6; 0.4]	**1.6E-4**
	$D_{2\%}$	102.9 ± 1.0	104.0 ± 0.9	−1.2 ± 1.1	[−3.5; 0.9]	**1.0E-3**
Kidney contralateral	$D_{50\%}$	23.8 ± 10.5	9.8 ± 10.5	14.1 ± 9.1	[0.9; 37.6]	**2.6E-4**
	$D_{2\%}$	70.8 ± 22.6	62.2 ± 26.0	8.6 ± 9.4	[−3.3; 35.5]	0.3
Kidney ipsilateral	$D_{50\%}$	57.7 ± 26.2	48.5 ± 29.5	9.2 ± 5.2	[0.2; 17.6]	0.4
	$D_{2\%}$	95.2 ± 17.3	94.2 ± 19.0	0.9 ± 2.1	[−1.5; 5.4]	0.8
Liver	$D_{50\%}$	26.4 ± 13.1	0.3 ± 0.9	26.1 ± 12.7	[1.0; 49.7]	**7.6E-8**
	$D_{2\%}$	81.6 ± 16.9	67.3 ± 28.5	14.4 ± 13.6	[−0.7; 38.8]	0.2
Spleen	$D_{50\%}$	32.3 ± 32.8	17.7 ± 34.1	14.6 ± 10.5	[−1.3; 35.4]	**1.1E-3**
	$D_{2\%}$	65.2 ± 37.0	58.1 ± 43.8	7.2 ± 9.5	[−3.0; 25.1]	0.7
Pancreas	$D_{50\%}$	83.4 ± 22.8	66.8 ± 31.6	16.6 ± 17.1	[−0.8; 55.6]	**4.4E-2**
	$D_{2\%}$	98.7 ± 10.0	96.7 ± 21.6	1.9 ± 11.7	[−4.0; 51.1]	0.2
NT	V_{2Gy}	34.0 ± 8.8	14.2 ± 5.0	19.8 ± 5.2	[12.7; 30.2]	**1.4E-7**
	$V_{95\%}$	4.2 ± 2.1	3.8 ± 1.8	0.4 ± 0.6	[−0.7; 1.7]	0.6

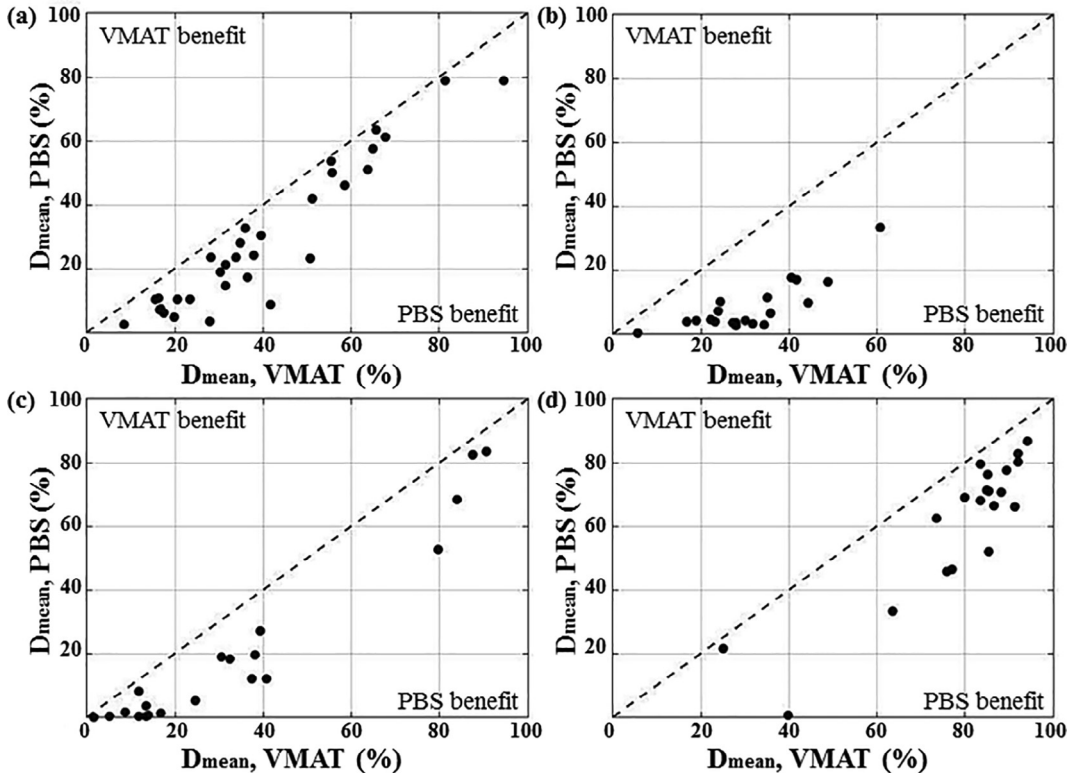

Fig. 2. D_{mean} delivered by VMAT and PBS to the OARs for the kidneys (a), liver (b), spleen (c) and pancreas (d).

methods. Being aware that photon planning is commonly done using a PTV approach, differences between PTV-based and ITV-based robustly optimized VMAT dose distributions were calculated (Supplementary material). No significant deviations were found for the majority of the DVH parameters. In addition, a realistic choice of set-up and range (only for PBS) uncertainties was aimed during the robust optimization and evaluation [13,25]. However, it can still be argued if the chosen uncertainties are too large given the available online image guidance and verification techniques. In previous studies [20,37], we estimated the target safety margin to use in a CBCT-guided workflow for a group of 15 WT patients. When accounting for the treatment chain geometric accuracy, patient set-up and inter-fraction motion uncertainties, a target safety margin of 5 mm in all orthogonal directions was calculated [37]. For this reason, a 5 mm set-up uncertainty plus an ITV margin to account for the breathing motion were used in this study. Nevertheless, range uncertainties might be further mitigated by the use of dual-energy CT [38] and/or proton CT [39].

In literature, 4D robustly optimized and evaluated PBS dose distributions are reported to be more robust and interplay-effect-resistant for moving targets than 3D robustly optimized dose distributions [40]. Since the use of 4D robust optimization and evaluation implies more manual work and optimization time, in the present work a 3D robust optimization and evaluation of the PBS dose distributions was performed. In addition, a 4D evaluation of the 3D robustly optimized PBS dose distribution for the patient denoting the largest breathing motion was done. For this patient, the target criterion ($V_{95\%} > 98\%$ in the Vw_{min}) was met for both

Table 2
Dose differences (ΔD) between planned and CBCT accumulated dose distributions for VMAT and PBS, with $p < 0.05$ (Wilcoxon signed-rank test) considered significant (in bold). Values are presented as a percentage of the respective PD. If $\Delta D > 0$ the planned dose is higher than the accumulated dose and $\Delta D < 0$ otherwise. *Abbreviations: SD = standard deviation.*

Structures	Parameter	ΔD (VMAT, planned-accumulated)			ΔD (PBS, planned-accumulated)		
		mean ± SD (%)	range (%)	*p*	mean ± SD (%)	range (%)	*p*
ITV	$D_{98\%}$	0.5 ± 0.9	[−1.9; 2.6]	**3.4E-2**	0.2 ± 0.5	[−0.3; 0.7]	0.7
	$D_{50\%}$	0.1 ± 0.8	[−2.4; 1.3]	0.2	0.1 ± 0.1	[−0.1; 0.3]	0.2
	$D_{2\%}$	−0.2 ± 0.9	[−2.8; 1.3]	0.6	−0.1 ± 0.6	[−1.7; 0.5]	1.0
Kidney contralateral	$D_{50\%}$	−0.2 ± 1.3	[−3.7; 2.6]	1.0	−0.2 ± 0.4	[−1.2; 0.4]	0.9
	$D_{2\%}$	−0.8 ± 3.5	[−9.4; 5.5]	0.9	0.0 ± 1.3	[−2.4; 4.2]	1.0
Kidney ipsilateral	$D_{50\%}$	1.9 ± 3.6	[−1.7; 9.6]	0.9	−0.1 ± 0.8	[−1.7; 1.2]	1.0
	$D_{2\%}$	0.0 ± 1.1	[−2.7; 1.9]	1.0	0.2 ± 0.6	[−0.2; 1.9]	0.8
Liver	$D_{50\%}$	0.4 ± 0.8	[−0.1; 2.6]	0.8	−0.2 ± 0.7	[−3.2; 0.1]	0.7
	$D_{2\%}$	0.6 ± 1.6	[−2.5; 4.8]	0.9	0.5 ± 2.5	[−4.8; 5.2]	1.0
Spleen	$D_{50\%}$	0.1 ± 0.8	[−1.7; 2.1]	1.0	0.2 ± 0.8	[−0.5; 3.4]	0.9
	$D_{2\%}$	−0.6 ± 3.0	[−11.3; 3.3]	0.8	0.0 ± 1.0	[−3.4; 1.6]	0.9
Pancreas	$D_{50\%}$	0.6 ± 1.5	[−1.9; 3.5]	0.9	0.6 ± 2.6	[−5.3; 4.7]	1.0
	$D_{2\%}$	0.1 ± 1.2	[−2.4; 2.3]	0.9	0.1 ± 1.0	[−2.2; 2.2]	0.6
NT	V_{2Gy}	0.7 ± 0.8	[−0.1; 3.0]	0.7	−0.1 ± 0.4	[−0.9; 0.9]	0.9
	$V_{95\%}$	0.1 ± 0.3	[−0.6; 0.8]	1.0	0.1 ± 0.1	[−0.1; 0.2]	0.8

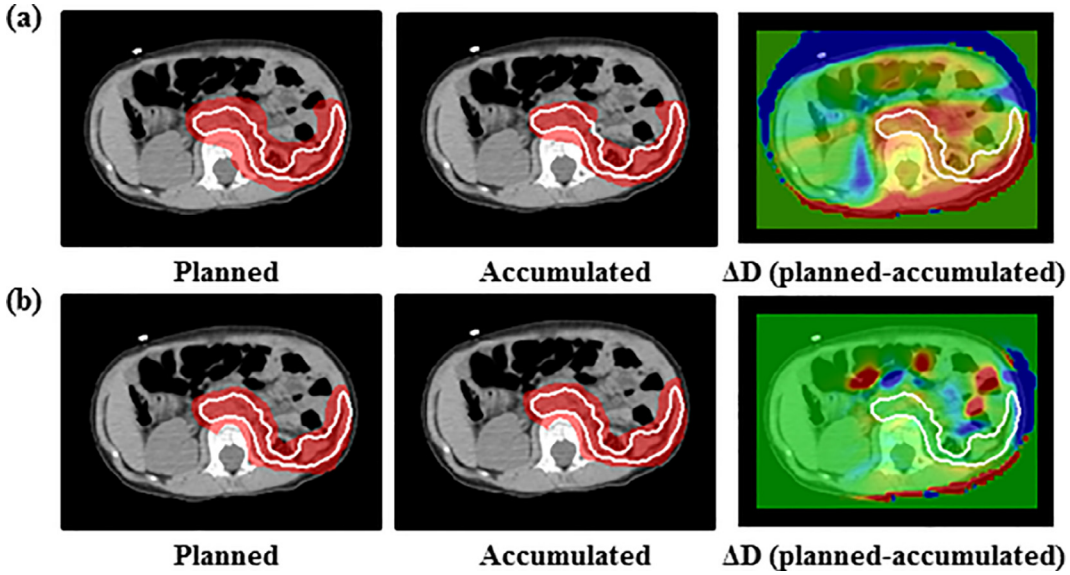

Fig. 3. VMAT (a) and PBS (b) planned and CBCT accumulated dose distributions for the patient failing the ITV coverage in the accumulated VMAT dose distribution. Dose distributions are overlaid on the planning-CT. The 95% isodose is shown in red and the ITV in white. ΔD denotes the dose difference between planned and CBCT accumulated dose distributions in a −0.5 (blue, planned < accumulated dose) to 0.5 (red, planned > accumulated dose) Gy range.

3D and 4D evaluation methods (98.9% vs. 99.8%). Due to the target posterior location, the beam configuration chosen and the small magnitude of the breathing motion seen for this patient group [20], using 3D robustly optimized and evaluated PBS dose distributions is considered clinically suitable. Moreover, plan robustness evaluation was performed using a Vw_{min} and not a worst-case dose as previously reported in literature [16,36]. Vw_{min} was chosen as a better agreement between the PTV criteria for photon plans and the target DVH criteria for PBS was denoted in comparison to the worst-case evaluation dose [26].

In this study, VMAT and PBS dose distributions robustness against inter-fraction anatomical changes was assessed using daily CBCT images. Due to the existence of possible image artifacts and inaccurate HUs, CBCT images are of limited value for direct dose calculations. Several methods to enable CBCT dose calculations have already been published in literature [31,41–43]. In the present work, the planning-CT was deformably registered to the CBCTs to calculate the fractional doses. Thus, two potential limitations of this approach are (1) the rigid accumulation of fractional doses and (2) the manual adaptation of daily gastrointestinal gas volume variations. For a deformable dose accumulation, a voxel-by-voxel accuracy is required [41] which cannot be ensured due to the poor CBCT image quality seen (Fig. 1). While using a rigid dose accumulation, daily anatomical deformations were neglected. Nevertheless, the largest inter-fraction anatomical changes, such as patient diameter and gastrointestinal gas volume variations, were accounted for. The manual adaptation of the gas volumes was sufficient for the purpose of this study but can represent a limitation for daily online re-planning. Due to the unpredictability of gastrointestinal gas volume changes, for the calculation of the fractional doses in abdominal cancer patients using a CBCT scatter correction approach as suggested by [43] or fast deep learning methods [44,45] might be considered better options for an online re-planning workflow. Nevertheless, these methods either require (1) storing of vendor specific CBCT projections [43], which is a disadvantage when needing to use other on-board imaging systems,

or (2) large amounts of imaging data [44,45], which is a limitation for children due to the large variability in age, height and weight in pediatric cohorts.

The results of this study show that the ITV coverage was reduced in the CBCT accumulated VMAT dose distribution compared to the planned dose for one patient. Smaller ITV and OARs dose differences were seen for PBS as a result of the selected beam configuration/angles. With the use of patient-specific posterior-oblique irradiation fields, uncertainties related to the variation of gastrointestinal gas volumes during treatment can be avoided as the proton beams stop before reaching the anterior part of the abdomen. Clinically, the VMAT plans are optimized using a full-arc as a requirement to achieve both an acceptable target coverage and a homogeneous dose in the vertebra [24]. Thus, planning strategies such as performing a density override of the gastrointestinal gas pockets on the planning-CT or using online daily re-planning might be necessary to reduce discrepancies between planned and delivered photon doses. In future studies investigating the robustness of both photon and proton radiotherapy plans, imaging data with more appropriate image quality should be used to better quantify the target and OARs fractional doses. Furthermore, the plan robustness evaluation should be included in trials to select patients that benefit from proton therapy. From a dosimetric point-of-view to treat children with WT or NBL, PBS showed to be more favorable, regarding both dose sparing and robustness against inter-fraction anatomical changes, compared to VMAT. Nevertheless, long-term follow-up of a large pediatric cohort is mandatory to estimate the real clinical benefit of treating children with PBS. In addition, a comprehensive dosimetric assessment of the available radiotherapy modalities is essential to take advantage of more recent techniques. In comparison with PBS, MRI-guided treatments are also showing to be promising for pediatric patients. With MRI-guided systems [46], the use of decreased safety margins due to the better visualization of the target could be achieved allowing for real-time adaptive regimes without extra patient radiation burden [47]. In a previous study [37], we have quantified the dosimetric impact when using MRI-guided IMRT ($IMRT_{MRI}$) compared to the clinical VMAT workflow to treat WT patients ($n = 15$). When using a PTV margin of 1 mm for the $IMRT_{MRI}$ (simulating a best-case scenario), the calculated D_{mean} was 18% in the kidneys, 30% in the liver, 32% in the spleen and 68% in the pancreas. In the present study, for the same patient category (WT, $n = 9$) when using robustly optimized intensity-modulated PBS dose distributions (5 mm, 3%), the computed D_{mean} was 15% in the kidneys, 10% in the liver, 32% in the spleen and 53% in the pancreas. Consequently for this patient category, PBS using current clinical robustness settings is shown to be more dosimetrically favorable compared to the best-case scenario of $IMRT_{MRI}$. In the future, further dosimetric sparing might be expected if using MRI-guided PBS (PBS_{MRI}). This approach is not clinically available yet, however research has been going on to prove the feasibility of MRI-guided proton systems and the corresponding treatment workflow [48]. Future work will include evaluating the potential dosimetric benefit with PBS_{MRI} for pediatric patients with abdominal tumors.

This study provides substantial dosimetric information to help assessing the optimal referral patterns for pediatric patients with abdominal tumors. Whether the reported dosimetric gain and robustness against inter-fraction anatomical changes of PBS dose distributions is translated into any clinical benefit for this patient category is however uncertain at present time.

Declaration of Competing Interest

None.

Appendix A. Supplementary data

Supplementary data to this article can be found online at https://doi.org/10.1016/j.radonc.2019.06.025.

References

[1] Brok J, Treger TD, Gooskens SL, van den Heuvel-Eibrink MM, Pritchard-Jones K. Biology and treatment of renal tumours in childhood. Eur J Cancer 2016;68:179–95.

[2] Maris JM, Hogarty MD, Bagatell R, Cohn SL. Neuroblastoma. Lancet 2007;369:2106–20.

[3] Pritchard-Jones K, Bergeron C, de Camargo B, van den Heuvel-Eibrink MM, Acha T, Godzinski J, et al. Omission of doxorubicin from the treatment of stage II-III, intermediate-risk Wilms' tumour (SIOP WT 2011): an open-label, non-inferiority, randomised controlled trial. Lancet 2015;386:1156–64.

[4] Ladenstein R, Pötschger U, Pearson ADJ, Brock P, Luksch R, Castel V, et al. Busulfan and melphalan versus carboplatin, etoposide, and melphalan as high-dose chemotherapy for high-risk neuroblastoma (HR-NBL1/SIOPEN): an international, randomised, multi-arm, open-label, phase 3 trial. Lancet 2017;18:500–14.

[5] Otto K. Volumetric modulated arc therapy: IMRT in a single gantry arc. Med Phys 2008;35:310–7.

[6] Lomax AJ. Intensity modulation methods for proton radiotherapy. Phys Med Biol 1999;44:185–205.

[7] Lomax AJ, Bohringer T, Bolsi A, Coray D, Emert F, Gotein G, et al. Treatment planning and verification of proton therapy using spot scanning: initial experiences. Med Phys 2004;31:3150–7.

[8] Hill-Kayser C, Tochner Z, Yimei L, Kurtz G, Lustig RA, James P, et al. Outcomes after proton therapy for treatment of pediatric high-risk neuroblastoma. Int J Radiat Oncol Biol Phys 2019;104:401–8.

[9] Hillbrand M, Georg D, Gadner H, Potter R, Dieckmann K. Abdominal cancer during early childhood: a dosimetric comparison of proton beams to standard and advanced photon radiotherapy. Radiother Oncol 2008;89:141–9.

[10] Hattangadi JA, Rombi B, Yock TI, Broussard G, Friedmann AM, Huang M, et al. Proton radiotherapy for high-risk pediatric neuroblastoma: early outcomes and dose comparison. Int J Radiat Oncol Biol Phys 2011;83:1015–22.

[11] Kristensen I, Nilsson K, Nilsson P. Comparative proton and photon treatment planning in pediatric patients with various diagnoses. Int J Particle Ther 2015;2:367–75.

[12] Vogel J, Lin H, Both S, Tochner Z, Balis F, Hill-Kayser C. Pencil beam scanning proton therapy for treatment of retroperitoneum after nephrectomy for Wilms tumor: a dosimetric comparison study. Pediatr Blood Cancer 2017;64:39–45.

[13] Albertini F, Hug EB, Lomax AJ. Is it necessary to plan with safety margins for actively scanned proton therapy? Phys Med Biol 2011;56:4399–413.

[14] Fredriksson A, Forsgren A, Hårdemark B. Minimax optimization for handling range and setup uncertainties in proton therapy. Med Phys 2011;38:1672–84.

[15] Unkelbach J, Chan TCY, Bortfeld T. Accounting for range uncertainties in the optimization of intensity modulated proton therapy. Phys Med Biol 2007;52:2755–73.

[16] Stuschke M, Kaiser A, Pöttgen C, Lubcke W, Farr J. Potentials of robust intensity modulated scanning proton plans for locally advanced lung cancer in comparison to intensity modulated photon plans. Radiother Oncol 2012;104:45–51.

[17] Stuschke M, Kaiser A, Abu-Jawad J, Pöttgen C, Levegrün S, Farr J. Multi-scenario based robust intensity-modulated proton therapy (IMPT) plans can account for set-up errors more effectively in terms of normal tissue sparing than planning target volume (PTV) based intensity-modulated photon plans in the head and neck region. Radiat Oncol 2013;8:145.

[18] Borgefors G. Hierarchical chamfer matching: a parametric edge matching algorithm. Pattern Anal Mach Intell IEEE Trans 1988;10:849–65.

[19] Elekta AB. Elekta synergy clinical user manual XVI R5.0. Stockholm: Elekta; 2013.

[20] Guerreiro F, Seravalli E, Janssens GO, van de Ven CP, van den Heuvel-Eibrink MM, Raaymakers BW. Intra- and inter-fraction uncertainties during IGRT for Wilms' tumor. Acta Oncol 2018;57:941–9.

[21] RaySearch Laboratories. RSL-D-61-217 RayPhysics 4.5 user manual. Stockholm, Sweden: RSL; 2014.

[22] Paganetti H. Relative biological effectiveness (RBE) values for proton beam therapy. Variations as a function of biological endpoint, dose, and linear energy transfer. Phys Med Biol 2014;59:419–72.

[23] Taylor PA, Kry SF, Followill DS. Pencil beam algorithms are unsuitable for proton dose calculations in lung. Int J Radiat Oncol 2017;99:750–6.

[24] Hoeben BA, Carrie C, Timmermann B, Mandeville HC, Gandola L, Dieckmann K, et al. Management of vertebral radiotherapy dose in paediatric patients with cancer: consensus recommendations from the SIOPE radiotherapy working group. Lancet Oncol 2019;20:155–66.

[25] Moyers MF, Sardesai M, Sun S, Miller DW. Ion stopping powers and CT numbers. Med Dosim 2010;35:179–94.

[26] Korevaar EW, van Dijk LV, Kierkels RG, Sijtsema NM, Bijl HP, Langendijk JA, et al. Evaluation of robustness of target coverage: transition from the PTV concept to multi-scenario CTV evaluation. Proceedings of the 55th annual meeting for the Particle Therapy Cooperative Group (PTCOG), 2016.

[27] Lomax A. SFUD, IMPT, and plan robustness. In: Rath A, Sahoo N, editors. Particle radiotherapy. Springer; 2016. p. 169–94.
[28] Ribeiro CO, Meijers A, Korevaar EW, Muijs CT, Both S, Langendijk JA, et al. Comprehensive 4D robustness evaluation for pencil beam scanned proton plans. Radiother Oncol 2019;136:185–9.
[29] Stock M, Pasler M, Birkfellner W, Homolka P, Poetter R, Georg D. Image quality and stability of image-guided radiotherapy (IGRT) devices: a comparative study. Radiother Oncol 2009;93:1–7.
[30] Fotina I, Hopfgartner J, Stock M, Steininger T, Lütgendorf-Caucig C, Georg D. Feasibility of CBCT-based dose calculation: comparative analysis of HU adjustment techniques. Radiother Oncol 2012;104:249–56.
[31] Veiga C, McClelland J, Moinuddin S, Lourenco A, Ricketts K, Annkah J, et al. Toward adaptive radiotherapy for head and neck patients: feasibility study on using CT-to-CBCT deformable registration for 'dose of the day' calculations. Med Phys 2014;41:031703.
[32] de Senneville BD, Zachiu C, Ries M, Moonen CTW. Evolution: an edge-based variational method for non-rigid multi-modal image registration. Phys Med Biol 2016;61:7377–96.
[33] Zachiu C, de Senneville BD, Tijssen RHN, Kotte ANTJ, Houweling AC, Kerkmeijer LGW, et al. Non-rigid CT/CBCT to CBCT registration for online external beam radiotherapy guidance. Phys Med Biol 2017;63:015027.
[34] Lomax AJ. Intensity modulated proton therapy and its sensitivity to treatment uncertainties 1: the potential effects of calculational uncertainties. Phys Med Biol 2008;53:1027–42.
[35] Lomax AJ. Intensity modulated proton therapy and its sensitivity to treatment uncertainties 2: the potential effects of inter-fraction and inter-field motions. Phys Med Biol 2008;53:1043–56.
[36] Liu W, Frank SJ, Li X, Zhu RX, Mohan R. PTV-based IMPT optimization incorporating planning risk volumes vs robust optimization. Med Phys 2013;40:021709.
[37] Guerreiro F, Seravalli E, Janssens GO, van den Heuvel-Eibrink MM, Lagendijk JJW, Raaymakers BW. Potential benefit of MRI-guided IMRT for flank irradiation in pediatric patients with Wilms' tumor. Acta Oncol 2019;58:243–50.
[38] Yang M, Virshup G, Clayton J, Zhu XR, Mohan R, Dong L. Theoretical variance analysis of single-and dual-energy computed tomography methods for calculating proton stopping power ratios of biological tissues. Phys Med Biol 2010;55:1343–62.
[39] Hansen DC, Seco J, Sørensen TS, Petersen JB, Wildberger JE, Verhaegen F, et al. A simulation study on proton computed tomography (CT) stopping power accuracy using dual energy CT scans as benchmark. Acta Oncol 2015;54:1638–42.
[40] Liu W, Schild SE, Chang JY, Liao Z, Chang Y-H, Wen Z, et al. Exploratory study of 4D versus 3D robust optimization in intensity modulated proton therapy for lung cancer. Int J Radiat Oncol 2016;95:523–33.
[41] Veiga C, Lourenço AM, Mouinuddin S, van Herk M, Modat M, Ourselin S, et al. Toward adaptive radiotherapy for head and neck patients: uncertainties in dose warping due to the choice of deformable registration algorithm. Med Phys 2015;42:760–9.
[42] Kurz C, Dedes G, Resch A, Reiner M, Ganswindt U, Nijhuis R, et al. Comparing cone-beam CT intensity correction methods for dose recalculation in adaptive intensity-modulated photon and proton therapy for head and neck cancer. Acta Oncol 2015;54:1651–7.
[43] Kurz C, Kamp F, Park YK, Zollner C, Rit S, Hansen D, et al. Investigating deformable image registration and scatter correction for CBCT-based dose calculation in adaptive IMPT. Med Phys 2016;43:5635–46.
[44] Kida S, Nakamoto T, Nakano M, Nawa K, Haga A, Kotoku JI, et al. Cone beam computed tomography image quality improvement using a deep convolutional neural network. Cureus 2018;10:2548.
[45] Kurz C, Hansen DC, Savenije MH, Landry G, Maspero M, Kamp F, et al. Cone-beam CT intensity correction for adaptive radiotherapy of the prostate using deep learning [OA127]. Phys Medica 2018;52:48.
[46] Raaymakers BW, Jürgenliemk-Schulz IM, Bol GH, Glitzner M, Kotte ANTJ, van Asselen B, et al. First patients treated with a 1.5T MRI-Linac: clinical proof of concept of a high-precision, high-field MRI guided radiotherapy treatment. Phys Med Biol 2017;62:41–50.
[47] Lagendijk JJW, Raaymakers BW, Van den Berg CAT, Moerland MA, Philippens ME, van Vulpen M. MR guidance in radiotherapy. Phys Med Biol 2014;59:349–69.
[48] Oborn BM, Dowdell S, Metcalfe PE, Crozier S, Mohan R, Keall PJ. Future of medical physics: real-time MRI-guided proton therapy. Med Phys 2017;44:77–90.